Int J Fract (2006) 139: 495–508
DOI 10.1007/s10704-006-0052-0

ORIGINAL ARTICLE

# Microstructure and fracture mechanical response of wood

**Stefanie E. Stanzl-Tschegg**

Received: 31 October 2005 / Accepted: 27 February 2006


**Abstract** Investigations on the fracture properties of wood in relation to its microstructure are reported. The inhomogeneous and hierarchical structure of wood is addressed. Wood species, the influence of orientation, the role of structural features, like rays are considered and discussed. Likewise the mode of loading, which determines the mode of fracturing, and the influence of humidity have been studied by using new fracture mechanical techniques and ways of evaluation. The specific fracture energy has been determined under crack opening conditions. In-situ loading in an environmental scanning electron microscope (ESEM), which allows observation in moistured condition, has been performed in order to investigate the mechanisms of fracturing of wood on a sub-microscopic scale. In the nanometer range, especially the influence of the microfibril angle on deformation and fracture behaviour has been studied.

**Keywords** Microstructure · Fracture · Fracture energy · Wood

S.E. Stanzl-Tschegg (✉)
Institute of Physics and Materials Science, Christian Doppler Laboratory for Fundamentals of Wood Machining, Department of Material Sciences and Process Engineering, BOKU — University of Natural Resources and Applied Life Sciences Vienna, Austria
e-mail: stefanie.tschegg@boku.ac.at

## 1 Introduction

Wood is a highly anisotropic and complex material. Therefore it has to be assumed that also fracturing is a complex process, which needs more sophisticated methods for its quantitative characterization than fracture mechanical procedures, which have been developed for homogeneous materials like metals. Since more than 30 years, this problem has been addressed (Schniewind and Pozniak 1971, Jeronimidis 1980; Boatright and Garrett 1983). It has been pointed out, for example, that in front and around the crack tip strain softening process zones are generated in wood, which are in contrast to the assumptions of linear elastic fracture mechanics (LEFM) principles (Aicher and Reinhardt 1993). In addition, the anisotropic, i.e. orthotropic structure of wood makes application of LEFM methods difficult, so that modeling with use of FEM is necessary and has been developed (Stanzl-Tschegg et al. 1995).

It has been shown that application of LEFM is a useful tool to characterize crack initiation of wood, i.e. the onset of fracturing in many cases. This fact is caused by the linear elastic behavior of wood up to relatively high loads, due to the rather high stiffness with negligible irreversible deformation of wood. A typical LEFM parameter is the fracture toughness $K_{IC}$, which characterizes the maximum load which is endured by the material before a crack starts. Another specific

property is the slope of the load–displacement diagram, termed $k_{init}$ in the following, which is proportional to the elastic modulus and characterizes the deformation behavior before crack initiation. These two parameters can be determined with conventional LEFM procedures. The crack propagation phase, however, cannot be characterized with these standard-testing methods, as stable crack propagation is required and usually cannot be obtained. The wedge splitting technique according to Tschegg (1986) makes it possible, and useful information may be derived from the recorded load-displacement diagrams. Especially the specific fracture energy $G_f$ is an important material characterizing parameter, and results are reported in the following.

Several materials related properties play an important role and determine the mechanical and fracture properties on a macroscopic as well as on a microscopic scale. Among these are wood species, year ring structure, fiber orientation, rays and mass density distribution, but also submicroscopic features, like cell wall structure and microfibril angle and the polymer assembly of the cells. In addition influences from outside, like humidity, temperature or mode of loading are influencing the deformation and fracturing processes of wood and must be considered.

Today's advanced testing techniques, like environmental scanning microscopy together with in-situ deformation experiments allow obtaining more insight into the structural features and mechanisms, being responsible for the different fracture processes of wood in the sub-microscopic range. Some more recent investigations will be reported in the following. They refer to these new testing techniques as well as to results correlating measured characteristic quantitative parameters with observations of fracture processes on different levels of magnification.

## 2 Determination of fracture toughness $K_{IC}$ and specific fracture energy $G_f$ in the crack opening mode (mode I)

The fracture behavior of wood in the crack opening mode (mode I) may be characterized by using the wedge splitting technique (Tschegg 1986). This has been developed for inhomogeneous materials and does not only allow to determine the fracture toughness $K_{IC}$, as a linear elastic material parameter, but also the fracture energy G, which is needed to split a specimen completely. In order to obtain $K_{IC}$, the maximum load has to be measured, whereas the whole load–displacement curve has to be recorded in order to obtain $G$. This is possible with the wedge splitting technique, which makes stable crack propagation possible. $G$ is calculated from the area integral below the recorded load–displacement curve. The testing procedure is described shortly in the following (Fig. 1). A wedge is pressed against load transmission pieces of the specimen in a standard material-testing machine. Friction is minimized by the use of roll bodies.

The horizontal splitting force $F_H$ is obtained from the force of the testing machine $F_M$ and the wedge angle $\alpha$:

$$F_H = F_M/2\tan(\alpha/2).$$

The crack mouth opening displacement $\delta$ is measured with inductive displacement gauges mounted on the specimens on both sides of the starter notch.

The measured load–displacement curve (LDD) characterizes the whole fracture process (Fig.1b, Tschegg et al. 1999). Three basic parameters may be derived:

(i) The initial slope of the load–displacement curves in the linear elastic region $k_{init}$ characterizes the elastic response of the specimen and its stiffness.
(ii) The critical stress intensity factor $K_{IC}$ characterizes the maximum stress state and is derived from the maximum force $F_C$ (obtained from maximum $F_M$), which is necessary to start a crack:

$$K_{IC} = F_C a^{-3/2} Y(a/W, B, H)$$

$Y$ is a factor depending on the geometry, in particular the length of the starter notch $a$, the sample thickness $B$ and the sample height $W$. This equation is valid for isotropic materials only. In order to determine the critical stress intensity factor considering the orthotropic nature of wood the maximum horizontal splitting forces are taken as input

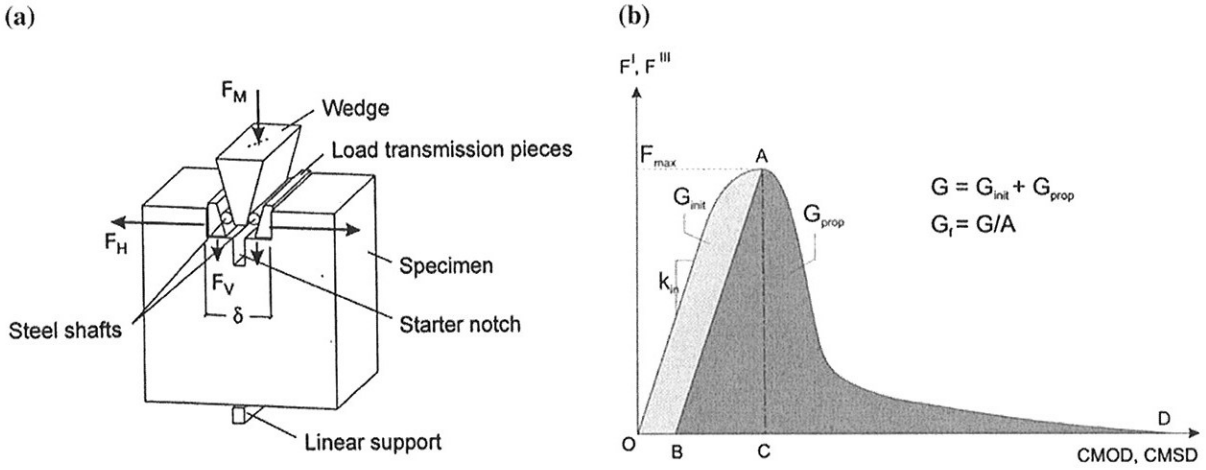


**Fig. 1** (**a**) Principle of wedge splitting technique (Tschegg 1986), (**b**) Energy contributions during the fracture process (Ehart et al. 1996)

data for a two-dimensional finite element simulation using quarter point elements and appropriate software (Stanzl-Tschegg et al. 1995).

(iii) The specific fracture energy $G_f$ is obtained from the integrated area under the load–displacement curve divided by the fracture area $A$:

$$G_f = \frac{1}{A} \int_0^{\delta \max} F_H(\delta) d\delta$$

It characterizes the whole Mode I fracture process until the specimen is split into two parts and does not depend on specimen size and shape if the specimen size is large enough (Stanzl-Tschegg et al. 1995).

In order to distinguish between crack initiation and propagation as to their energy consumption, the recorded area below the LDD diagram may be subdivided into two parts (Ehart et al. 1996) (Fig. 1b). The first part is the crack initiation energy $G_{init}$, which is dissipated in the crack initiation phase. This energy is needed to form microcracks (and smaller irreversible deformations) leading to the generation of a macrocrack. It is proportional to the area under the tangential line to the origin of the curve and a parallel line going through the maximum load of the LDD (area below O-A-B-O) according to the "plastic model" (Ehart et al. 1996). The second part, that is consumed after the load maximum is reached, is the energy which is necessary to propagate the crack ($G_{prop}$). It may be obtained by subtraction of $G_{init}$ from the total fracture energy $G_f$. $G_{prop}$ consists of the elastically stored energy in the specimen after the begin of macroscopic crack propagation (B-A-C-B in Fig. 1b) and the remaining area under the LDD (C-A-D-C). The elastically stored energy is dissipated during crack propagation.

All experiments described in the following were performed with specimens of 12% moisture content, after conditioning in a climate chamber of 65% relative humidity at 20°C (besides experiments describing the influence of different moisture content).

## 2.1 Load–displacement curves of different wood species (hardwood and softwood)

In order to specify the fracture properties of different wood species, four species with different microstructure have been tested under mode I loading perpendicular to the grain (Reiterer et al. 2002a): one softwood, spruce (*Picea abies* [L.] Karst.) and three hardwoods, alder (*Alnus glutinosa* Gaertn.), oak (*Quercus robur* L.) and ash (*Fraxinus excelsior* L.).[1] Softwood like spruce consists of up to 95% tracheids oriented longitudinally parallel to

[1] In paranthesis: Latin names plus abbreviations of names: [L.] for C. Linne, Karst for Karstens and Gaertn. for Gaertner.

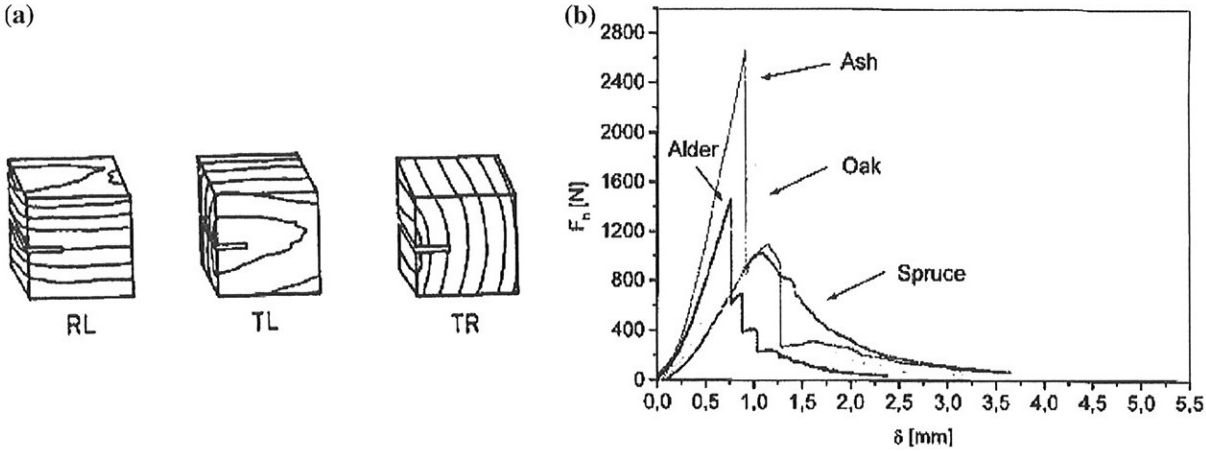


**Fig. 2** (**a**) Terminology of crack propagation orientation: RL, TL and TR, (**b**) load–displacement curves of different wood species obtained by the wedge splitting test in the RL system (Reiterer et al. 2002a)

the stem axis. Only 5–10% of the tissue are oriented in radial direction, the uniseriate rays. Hardwoods are more specialized in their structure consisting of different tissue types like vessels, fiber tracheids, libriform fibers and rays. Hardwoods may have larger rays (multiseriate rays) and a higher relative volume fraction of this radially oriented tissue.

The load–displacement curves were determined for the RL and TL crack propagation system (R and T, respectively, indicate the direction of the crack plane normal and L the direction of crack propagation, see Fig. 2a) of the four wood species. The curves of the RL system are reproduced in Fig. 2b. Spruce shows completely stable crack propagation and the load–displacement curves show a round maximum peak load and clear deviation from linear elastic behavior. Quite in contrast unstable crack propagation followed by several crack arrests is observed in the hardwoods. The maximum load in the load–displacement curves of the hardwoods is visible as sharp peaks, which is typical for linear elastic brittle materials. Moreover, less microcracks are formed during the crack initiation phase of the hardwoods, which has been verified using acoustic emission measurements (Reiterer et al. 2000). This different deformation and fracture behaviour of soft- and hardwood may be partially attributed to their different fiber structure. Hardwood fibers are shorter than spruce fibers and therefore energy dissipating processes like fiber bridging probably are less effective.

### 2.2 Dependence of $K_{IC}$ and $G_f$ on wood species, orientation and density

Figure 3a and b show the dependence of $K_{IC}$ and $G_f$ on the mean density of the four tested wood species. The critical stress intensity factors $K_{IC}$ indicating the resistance against crack initiation are higher in the RL system (Fig. 3a). A similar trend is observed for the initial slope in the load–displacement curve indicating the stiffness of the species (not shown in Fig. 3a) (Reiterer et al. 2002a). Critical stress intensity factors are generally higher for the hardwoods. The $K_{IC}$ values are lowest for spruce, in both the RL and TL system, and within the hardwoods ash has the highest $K_{IC}$ values. The values range from 0.49 to 1.16 $MPam^{1/2}$ in the RL and from 0.31 to 0.65 $MPam^{1/2}$ in the TL system.

Figure 3a demonstrates that $K_{IC}$ increases with increasing density of the four wood species. In both systems, linear regressions show excellent fits with regression coefficients of $R = 0.98$ for the RL and $R = 0.99$ for the TL system. The influence of density on $K_{IC}$values is in accordance with reported results by Schniewind et al. (1982), Petersson and Bodig (1983) and Gibson and Ashby (1997). Gibson and Ashby (1997) modeled wood as a cellular material and derived a relationship between density and $K_{IC}$ in the form $K_{IC} \sim \rho^{3/2}$. The results as plotted in Fig. 3a show a linear dependence of $K_{IC}$ on the density for the RL system ($K_{IC} \sim \rho$), but if they are plotted vs. $\rho^{3/2}$ a similar good relationship

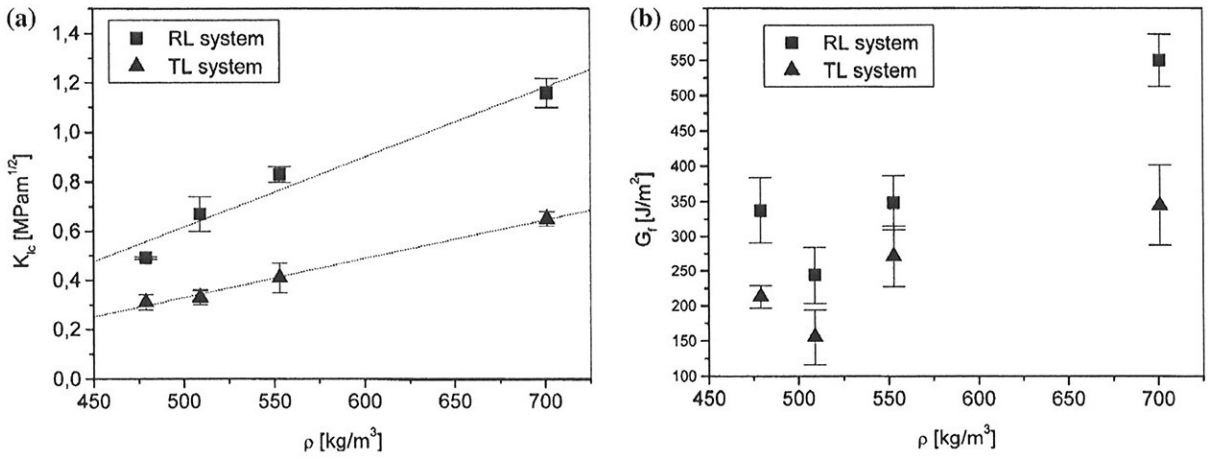


**Fig. 3** (**a**) Critical stress intensity factor $K_{IC}$ and (**b**) specific fracture energy $G_f$ of different wood species (from left to right: spruce, alder, oak, ash) (Reiterer et al. 2002a)

is obtained, and the results do not contradict the foam model. The differences between the different wood species (having different densities) are higher for the RL system, which results in a larger slope of the regression line.

The results for the specific fracture energy $G_f$, characterizing the entire fracture process until complete separation of the specimen, show a similar ranking within the hardwood species, but not if spruce (softwood) is included (Fig. 3b). In the RL system ash has the highest specific fracture energy and spruce and oak show almost identical values. The TL system shows quite similar results. In both systems alder reaches the lowest specific fracture energies of the tested hardwoods. The values vary from 244 to 550 J/m$^2$ in the RL system. The results demonstrate that the density alone cannot explain the different energy consumption of the fracture process, but that the above mentioned different fiber structure also plays a role.

### 2.3 Rays and their influence on fracture mechanical properties

In order to investigate the role of rays more extensively, additional studies were performed on oak (*Quercus robur* L.) and ash (*Fraxinus excelsior* L.) (Reiterer et al. 2002b). Both trees are ring-porous species, in terms of their structural biological characterization. Each growth ring consists of a less dense earlywood dominated by large vessels and a latewood dominated by fibers serving for the longitudinal (L) stiffness and strength of the wood in the living tree. A parameter of significant structural difference between the both tree species is the ray tissue characteristic. While ash consists of rather unique multiseriate and sturdy rays, for oak two types of rays can be distinguished; only a few very large rays with a height of 1mm or more and a high amount of very small uniseriate rays. Their cell wall structure is optimized to provide sufficient mechanical properties regarding the main loading conditions of the living tree (e.g. bending of the stem due to wind loads). In the transverse plane the radial (R) and the tangential (T) direction can be distinguished. The mechanical properties of wood in these directions are known to be an order of magnitude lower compared to the longitudinal. Comparing the radial and the tangential direction, the radial properties are higher than the tangential ones.

To investigate the fracture mechanical properties, the wedge splitting technique (Tschegg 1986) was used. The fracture mechanical results, i.e. the initial slope $k_{init}$, the critical Mode I stress intensity factor $K_{IC}$ and the specific fracture energy $G_f$ are shown in Fig. 4. The initial slope $k_{init}$ characterizes the elastic behavior and is proportional to an effective modulus of elasticity (Harmuth et al. 1996). Figure 4a shows that the stiffness in the RL system is higher than in the TL system for both

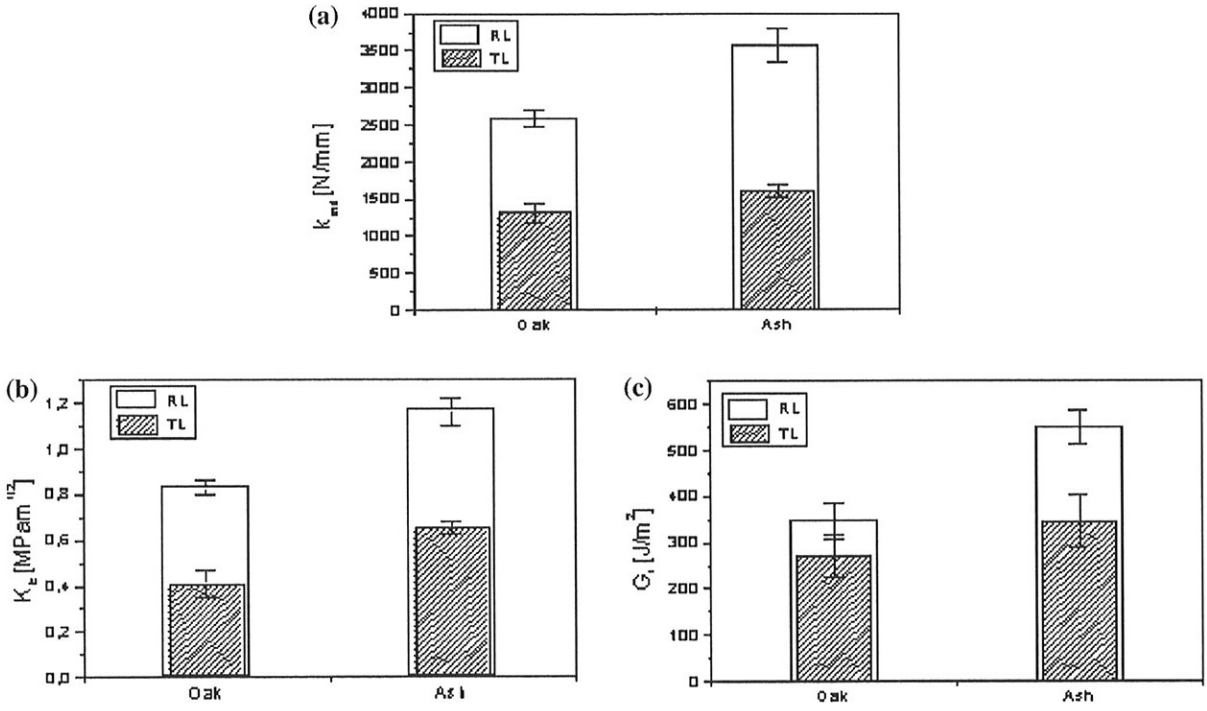


**Fig. 4** (**a**) Initial slope $k_{init}$, (**b**) critical stress intensity factor $K_{IC}$ and (**c**) specific fracture energy $G_f$ in the RL and TL propagation system of oak and ash (Reiterer et al. 2002a)

species. Ash shows higher initial slopes. For the TL system the differences between the wood species are lower. The initial slopes vary from 2.5 to 3.5 N/m in the RL system and from 1.3 to 1.6 N/m in the TL system.

From the maximum splitting forces the critical stress intensity factors $K_{IC}$ were determined considering the orthotropic nature of wood. The finite element simulation yielded the results shown in Fig. 4b. The $K_{IC}$ values are generally higher for ash than for oak and the differences between the two crack propagation systems are higher for ash.The results on the specific fracture energy $G_f$, characterizing the whole fracture process including crack initiation and propagation yield that ash has the highest specific fracture energy in both propagation systems (Fig 4c). For oak the values are more similar (350 J/m$^2$ in the RL and 270 J/m$^2$ in the TL system) than for ash (550 J/m$^2$ in the RL and 345 J/m$^2$ in the TL system).

Considering the structural differences, the significantly higher $G_f$ values in the RL orientation may be attributed to the rays. The sturdy rays of ash obviously are more efficient reinforcements in the RL orientation (Fig. 5). This result of rays acting as reinforcement in the RL crack propagation system is in accordance with the results on the mechanical properties of specimens without notch (Reiterer et al. 2002a). The rays carry tensile stresses in the developing process zone (containing microcracks and irreversibly deformed areas) around the crack tip before macrocrack initiation as well as during the crack propagation phase when the process zone is redeveloped and spreading through the material. In addition, it may be assumed that the rays act also as fiber reinforcement behind the crack tip during crack propagation consuming additional fracture energy. As the ratio between RL and TL systems is higher for the $K_{IC}$ values compared with the $G_f$ values, it may be concluded that the crack initiation phase is influenced more than the propagation phase.

### 2.4 Influence of moisture content on $K_{IC}$ and $G_f$

Wood, like any other biological material is able to adsorb and desorb water depending on the

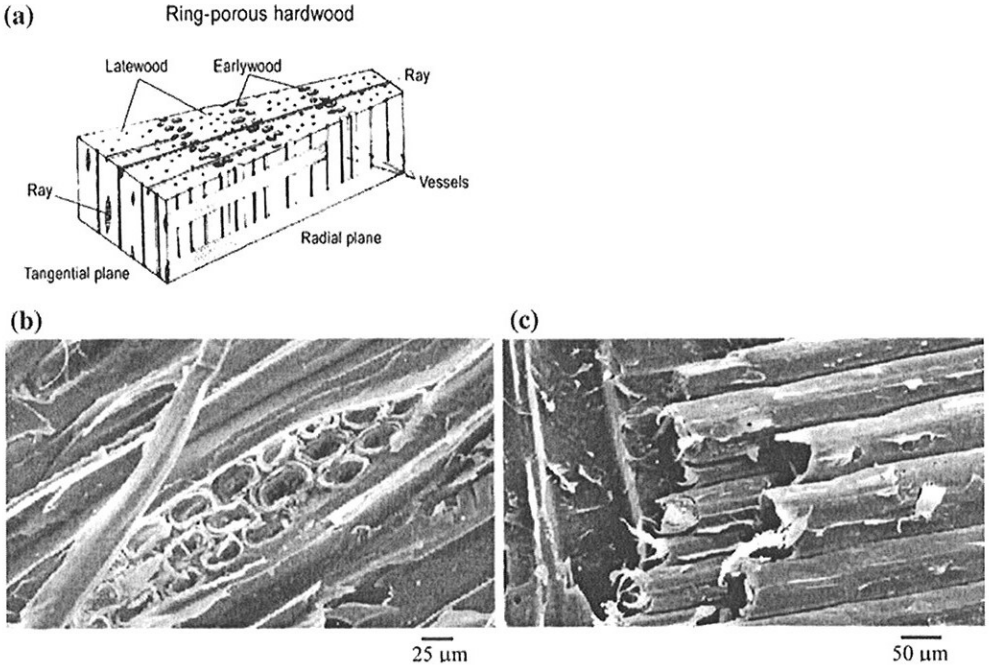


**Fig. 5** Typical features of anatomy of ring-porous hardwoods. (**a**) schematic drawing (Fengel and Wegener 2003 modified), (**b**), (**c**) SEM images of ash in the (**b**) RL and (**c**) TL crack propagation system (Reiterer et al. 2002b)

environmental conditions. It is well known that many wood properties are influenced by the moisture content (MC), which is defined as $MC = (m_{MC} - m_d)/100\,m_d$, where $m_{MC}$ is the mass at a certain MC and $m_d$ the mass in dried condition. In general, mechanical properties like stiffness or strength decrease with increasing moisture content (see for example Niemz 1993). Much less studies are available in the literature on the influence of moisture on the fracture properties than on the mechanical properties.

Therefore, mode I experiments were performed on spruce (*Picea abies* [L] Karst.) in the RL system using the wedge splitting technique at different MCs in order to determine the critical stress intensity factor and also non-linear fracture parameters like the specific fracture energy (Reiterer and Tschegg 2002). Notched specimens were prepared in the RL system such that the measured MCs for the differently stored series were (7±0.5)%, (12±0.7)%, (18±1)% and (55±5)%. Ten specimens were investigated for each moisture range. Their densities were in the range from 372 to 442 kg/m$^3$.

Typical load–displacement curves for the different moisture contents are shown in Fig. 6a. As can be seen the fracture behavior is clearly influenced by moisture. The curves indicate a decrease of the maximum stress and an increase of the displacements with increasing moisture content. The critical stress intensity factors $K_{IC}$ are shown in Fig. 6b. There is a significant decrease of $K_{IC}$ from moisture content of 7% to moisture content of 12% and less reduction from MC of 12% to MC of 55%. The results of the specific fracture energy $G_f$ are opposite. As shown in Fig. 6b, the specific fracture energy increases with increasing moisture content, which is in contrast to the decreasing $K_{IC}$.

Essentially two mechanisms are probably responsible for the higher specific fracture energies at higher MCs. One is the formation of the process zone around the crack tip (microcracks, irreversible deformations, etc) before the macrocrack starts to propagate, which needs more energy with increasing MC. Obviously dissipation of energy due to irreversible deformations is higher at higher MCs. Experimental evidence for the more ductile fracture at 55% MC is seen in Fig. 7b, which is

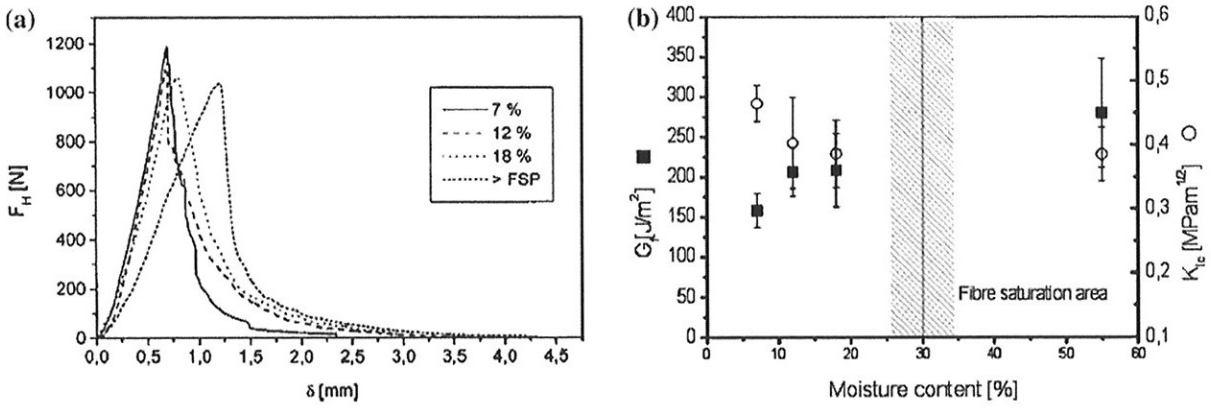


**Fig. 6** Moisture influence on (**a**) load–displacement curves, (**b**) specific fracture energy $G_f$ and criticial stress intensity factor $K_{IC}$ of sprucewood (error bars indicate standard deviation) (Reiterer and Tschegg 2002)

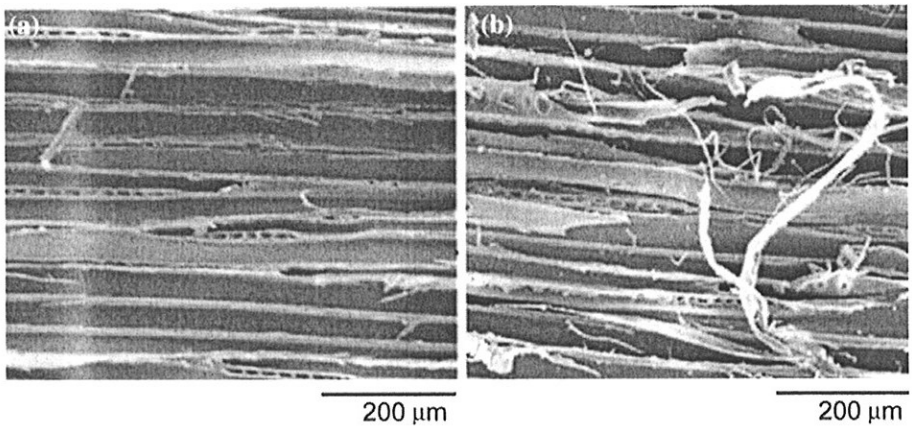


**Fig. 7** Typical fracture surface of spruce wood at (**a**) 17% moisture content and (**b**) 55% moisture content (Reiterer and Tschegg 2002)

in contrast with the more brittle one at 17% MC in Fig. 7a. Therefore, it may be assumed that the main reason for an increase of the specific fracture energy with increasing MC, especially compared to the saturated case, is an increase of irreversible deformation. The higher ductility overcompensates the reduction of the stiffness, and the maximum stress state leads in sum to an increased specific fracture energy. The second mechanism, which may increase $G_f$ at higher MC's, could be fiber bridging behind the crack tip during the final crack propagation phase, which consumes more energy if the material becomes more ductile.

This fracturing behavior may be modeled by means of the fictitious crack model (Hillerborg et al. 1976, Valentin et al. 1991; Boström 1994; Holmberg et al. 1999), using a bilinear strain softening curve and dividing it into the two parts, i.e. the one, where the energy is consumed to form a process zone (i.e. "microcracking" = part I) and that to bridge the already broken parts by fiber bridging (part II). The ratio of part II and part I becomes higher, if the fiber saturation point is reached and is in accordance with the experimental finding of a higher $G_f$ beyond the fiber saturation point, indicating an increased energy

dissipation due to fiber bridging processes (Reiterer and Tschegg 2002).

## 3 Correlation of fracture mechanical values with submicroscopic features

### 3.1 In-situ cracking in an ESEM

A better understanding environmental influences on the fracture process may be obtained by use of an environmental scanning electron microscope (ESEM) with an in-situ deformation stage. The combination of an ESEM with a cooling device makes observation in moistured condition possible. The simultaneous detection of load–displacement curves and crack propagation is a helpful approach to better understand the fracture behaviour of wood in relation to its structural characteristics.

Specimens of Norway spruce (*Picea abies* [L.] Karst.) were tensile loaded in longitudinal direction, with an initial notch cut along the R (−) direction (crack propagation from bark to pith) before attaching the specimen to the tensile device, thus resulting in crack propagation in the RL system (Frühmann et al. 2003; Burgert and Frühmann 2003). The geometry for microtensile specimens allowed complete fracture detection when testing wood parallel to the grain.

Figure 8 shows the load–displacement diagram of a specimen tested in-situ in the ESEM (Fig. 8a) and photographs of the fracture path at some specified stages of the load–displacement diagram (Figs. 8b–d). The arrows in Fig. 8a indicate the stages, where loading was interrupted to obtain ESEM images. Fig. 8b (08) shows that the crack is propagating essentially transversely through the earlywood, while the load reached about half of its maximum value. Close to the main crack very short tears appear above and below it. Fig. 8c (14) captured the moment when the crack path began to deviate, i.e. when the crack started to propagate along the latewood border. In Fig. 8d (19) deviation of the crack from the transverse plane downward along the latewood border has taken place already. The sequential reconstruction of the fracture process in a specimen loaded in LR by a mode I load demonstrates the principal differences of crack propagation in earlywood and latewood. In the less strong earlywood the fibers loaded in tension are mainly fractured transversely, whereas the thicker walled and stronger latewood fibers are mainly separated by shear failure resulting in a longitudinal crack path between the cells.

He and Hutchinson (1989) gave a theoretical explanation for the behavior of a crack entering a bimaterial interface. Although their theory was developed for linear elastic and isotropic materials, the basic idea is also applicable to wood with a crack propagating transversely in earlywood towards the growth ring border. The trajectory for the crack is determined by the ratio of the MOEs of the combined materials and the ratio of fracture toughnesses for a crack penetrating the interface vs. a crack propagating along the interface. Considering the high orthotropy of wood in the LR plane together with the remarkable difference in stiffness between earlywood and latewood, the crack is very likely deflected.

### 3.2 Correlation of work of fracture and nanostructure of the S2 cell wall

In order to obtain information on the nature of crack formation in wood on an even higher scale of magnification, tensile tests on spruce wood were combined with studies of the nanostructure of the S2 cell wall layer of the tracheids of Picea abies. There, especially knowledge of the microfibril angle was of interest, as it is known that the cellulose microfibril angle controls not only stiffness, but also the extensibility of wood. It was measured by means of the small angle X-ray technique (Jakob et al. 1994). These measurements were combined with tensile tests parallel to the grain. Tangential slices of spruce wood (Picea abies) were cut out of earlywood and latewood of the stem and two annual rings of the lower and upper side of the branch. In order to be able to correlate the deformation of the sample and their structure, the same specimens stressed in the tensile tests were used for investigation by small-angle X-ray scattering (SAXS) (Lichtenegger et al. 2000). The sample hydration was kept above the fiber saturation point.

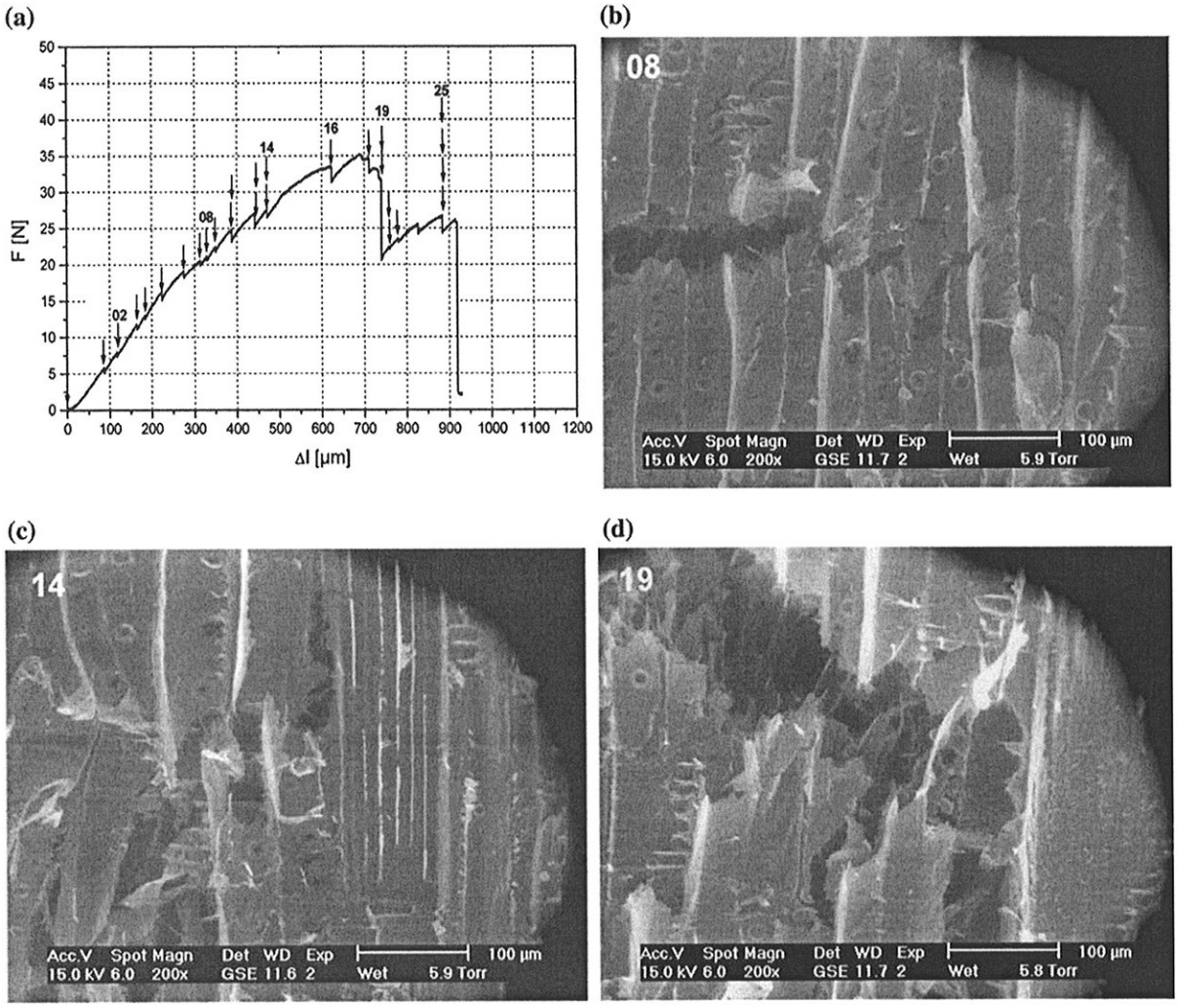


**Fig. 8** Load–displacement diagram obtained in-situ together with images in the ESEM. Arrows in 08, 14 and 19 in (**a**) indicate where the ESEM images in (**b**), (**c**), (**d**) were taken (Frühmann et al. 2003a)

From the SAXS measurements a microfibril angle of approximately 5° was obtained for earlywood of the stem, indicating an orientation of the cellulose fibrils roughly parallel to the longitudinal direction of the wood cell. In latewood samples, the microfibril angles were approximately 20°. In the branch higher microfibril angles were found, reaching 26° on the upper and 50° on the lower side. In Fig. 9 the longintudinal Young's modulus and the strain at maximum stress obtained from stress–strain curves are plotted as a function of the microfibril angle. For microfibril angles between less than 5° and 50°, the stiffness decreased by a factor of 10, and the ductility increased by a factor of 12.

In order to characterize the energy absorbing capacity during fracturing, the work of fracture $W_{\text{total}}$ of the investigated specimens was evaluated from the stress–strain curves (Reiterer et al. 2001). These curves show an abrupt decrease of the load from the maximum load after formation of the main macrocrack, which means that crack propagation was unstable. Therefore, the energy consumption due to crack propagation ($G_{\text{f}}$) cannot be detected in these experiments contrary to the wedge splitting experiments. The values $W_{\text{total}}$

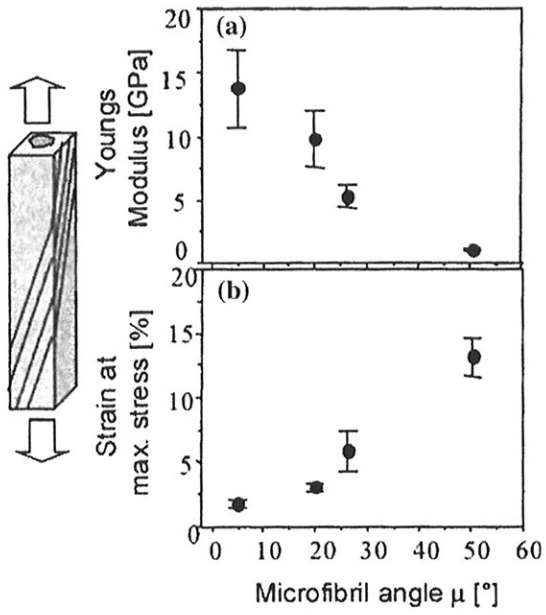


**Fig. 9** Influence of microfibril angle (MFA) on mechanical properties; (**a**) longintudinal Young's modulus, (**b**) maximum strain of the cell wall (Lichtenegger et al. 2000)

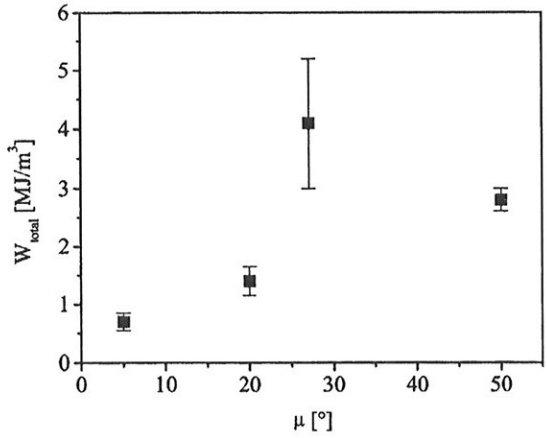


**Fig. 10** Total work of fracture at different microfibril angles $\mu$ (Reiterer et al. 2001)

characterize the consumed energy until onset of the final fracture. The results are plotted versus the microfibril angle in Fig. 10. As can be seen the absorbed energy during tensile loading increases with increasing microfibril angles and becomes maximum around 30–40°. For higher microfibril angles the energy absorption is mainly due to inelastic deformation. The fraction of absorbed energy due to elastic deformation is only approximately 10%.

Fractography of the tested specimens reflects the different energy absorbing capacity. In Fig. 11a the fracture zone of a wood specimen with a microfibril angle of about 5° is shown. The fracture surface is smooth and there are only few cell wall fragments visible indicating a brittle fracture process. Quite in contrast the fracture zone of wood specimens with a microfibril angle $\mu$ of appr. 55° (see Fig. 11b) shows a rough surface with highly deformed tracheids. Torn cell wall fragments spiraling out of the fractured tracheids indicate the ductile character of the fracture process.

In another study (Frühmann et al. 2003), wedge splitting experiments on spruce and beech were performed in-situ in the ESEM in the TR crack propagation system. Analysis of the results on specific fracture energy $G_f$, critical load (instead of the fracture toughness) and initial elasticity $k_{init}$, as well as the observations in the ESEM support the assumption that fracturing in wood in the TR system can be characterized by means of Linear Elastic Fracture Mechanics (LEFM). The heterogeneity of wood, however, must be considered. Two principal fracture mechanisms on the cell wall level have been observed: cell wall fracturing and intercellular cracking along the middle lamella. Ashby's et al. (1985) result of cell wall breaking being typical for low density wood (like in the early wood of spruce) and intercellular fracturing taking place preferentially in higher density wood (like in beech or in latewood of spruce) could be verified.

To obtain a deeper insight into the influence of micro-and nanostructure of deformation and fracture properties of wood, in-situ synchrotron experiments combined with microtensile loading–unloading experiments were performed not only on wood foils, but also on single cells. These experiments allow to correlate structural and mechanical characteristics at different stages of tensile loading. Fig. 12 shows the results on tissues (Figure 12a, b) and on single fibres (Fig. 12c, d). They demonstrate that the MFA decreases with increasing strain and stress in both cases (Keckes et al. 2004). Wood tissues exhibit a relatively high stiffness during the initial period of testing and a significantly lower one after a yield point has been exceeded. If straining is interrupted in this second regime (stress drops in Fig. 12a and c), the original stiffness is reached after reloading. Additional increase of the strain leads

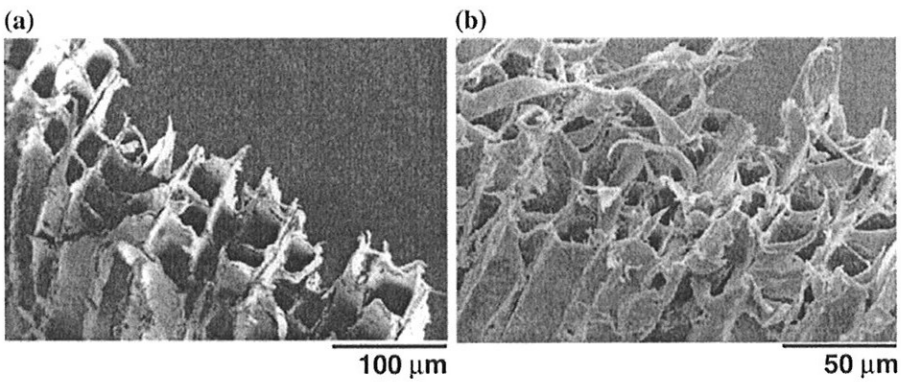


**Fig. 11** Fracture surfaces of specimens with different microfibril angles $\mu$; (**a**) $\mu \infty 5°$: rather smooth fracture surface, (**b**) $\mu \infty 55°$: strongly deformed and torn cell walls (Reiterer et al. 2001)

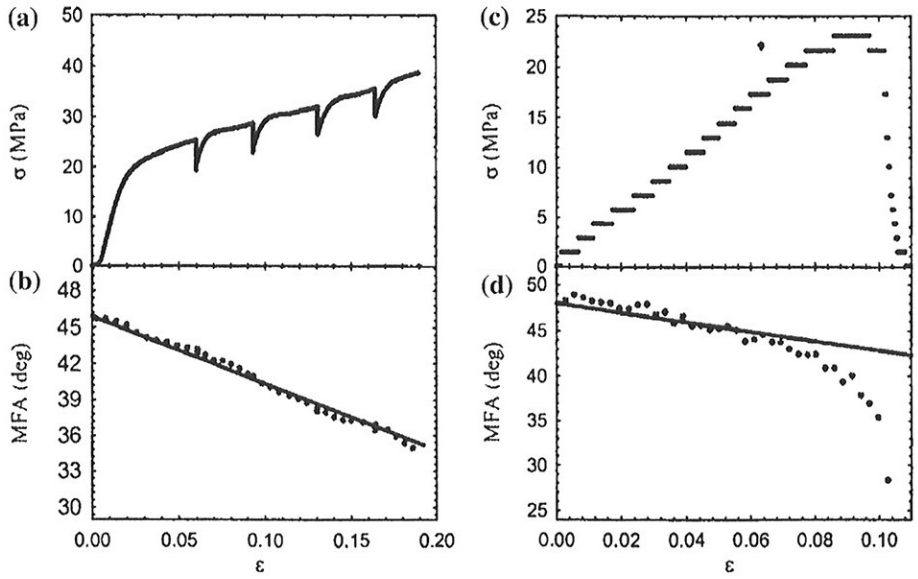


**Fig. 12** Mechanical and structural results from in-situ WAXS experiments on a (**a, b**) foil and single cell (**c, d**) of (**a**) stress–strain diagram curve with four interruptions of loading, (**b**) decrease of MFA with increasing strain. Solid line: theoretical prediction (Keckes et al. 2003). (**c d**) analogous results for single wood cells

to a curve with the original slope of the lower stiffness curve. This means that shear relaxation does not significantly damage the matrix. In-situ tests on single cells revealed a stress–strain curve without in initial steeper slope, but with a similar dependence of strain and stress on the MFA. Different from the deformation of the tissues, the deformation of the single cells was very inhomogenous along the length of the cell and, before the onset of fracture, the MFA decreased strongly (Fig. 12d).

These experimental data indicate that the MFA on one hand and an additional mechanism on the other hand is responsible for the stiffness recovery beyond the yield point, shown in Fig. 12a. It is supposed that there is a dominant recovery mechanism that re-forms the amorphous matrix between the cellulose microfibrils within the cell walls. This stick-slip mechanism acts like a Velcro connection, but on a nanometric level with molecular bonds. It is suspected that hemicelluloses being attached to the cellulose fibers give rise to this behaviour.

## 4 Conclusions

Several properties of wood have been investigated and reported in this overview, which are closely related to the specific microstructure of wood,

which is complex and hierarchical. Among these, the wood species and the orthotropic structure of wood have been considered as most essential. The fracture properties of different hard- and softwood species have been characterized with the wedge splitting technique according to Tschegg (1986) as a rather new fracture mechanical method and were correlated with the resulting fracture morphology. With this method, not only the fracture toughness $K_{IC}$, but also the specific fracture energy $G_f$, which is needed to completely separate a specimen, has been determined. Several parameters, which do not only determine the mechanical, but also the fracture properties, have been studied. Among these, the influence of mean density, of orientation, the role of rays as reinforcing elements in the sense of fracture mechanics and the effect of moisture content on fracture energy and fracture toughness have been investigated and quantified. The influence of moisture content was also studied by using an environmental scanning microscope (ESEM) together with an in-situ micro deformation stage, which allows to observe the fracture processes and to correlate them to the simultaneously measured applied loads and resulting displacements. Thus the mechanisms being responsible for the cracking process could be identified on a sub-microscopical level. On the nanometer level, the influence of the microfibril angle on deformation processes of thin wood foils and single cells as well as on the total work of fracture of solid wood was investigated.

## References


Aicher S, Reinhardt HW (1993) Einfluß der Bauteilgröße in der linearen und nichtlinearen (Holz-) Bruchmechanik. Holz als Roh- und Werkstoff 51:215–220

Ashby MF, Easterling KE, Harrysson R, Maiti SK (1985) The fracture and toughness of woods. Proc R Soc Lond 398:261–280

Boatright SWJ, Garrett GG (1983) The effect of microstructure and stress state on the fracture behaviour of wood. J Mat Sci 18:2181–2199

Boström L (1994) the stress-displacement relation of wood perpendicular to the grain. Part II. Application of the fictitious crack model to the compact tension specimen. Wood Sci Techn 319–327

Burgert I, Eckstein D (2001) The tensile strength of isolated rays of beech (Fagus sylvatica L.) and its significance for the biomechanics of living trees. Trees 15:168–170

Burgert I, Frühmann K (2003) Micromechanics of wood-surface-function relationships on the tissue and fiber level. In: Proc. Second Int. Conf ESWM, ed. STFI, Stockholm, Sweden, pp 85–94

Ehart RJA, Stanzl-Tschegg SE, and Tschegg EK (1996) Characterization of crack propagation in particle board. Wood Sci Techn 30:307–321

Fengel D and Wegener G (2003) Wood. Verlag Kessel, Remagen, D, www.forstbuch.de

Frühmann K, Burgert I, Stanzl-Tschegg SE (2003) Detection of the fracture path under tensile loads through in *situ* Tests in an ESEM Chamber. Holzforschung 57:326–332

Gibson LJ, Ashby MF (1997) Cellular solids. Cambridge Solid State Sci Ser 2nd edn, Cambridge University Press, Cambridge

Harmuth H, Rieder K, Krobath M, Tschegg EK (1996) Investigation of the nonlinear fracture behaviour of ordinary ceramic refractory materials. Mat Sci Eng A214, 53

He MJ, Hutchinson JW (1989) Crack deflection at an interface of dissimilar elastic materials. Int J Solids Struct 25:1053–1067

Hillerborg A, Modeer M, Petersson PE (1976) Analysis of crack formation and crack growth in concrete by means of fracture mechanics and finite elements. Cement Concrete Res 6:773–782

Jakob H, Fratzl P, Stanzl-Tschegg SE (1994) Size and arrangement of elementary cellulose fibrils in wood: a small-angle X-ray scattering study of Picea Abies. J Struct Biol 113:13–22

Jeronimidis G (1980) The fracture behaviour of wood and the relations between toughness and morphology. In: Proc. R. Soc Lond B 208, pp 447–460

Keckes J, Burgert I, Frühmann K, Müller M, Kölln K, Hamilton M, Burghammer M, Roth S, Stanzl-Tschegg S, Fratzl P (2003) Cell-wall recovery after irreversible deformation of wood. Nature Materials, 2, 811; publ. online: 16 Nov. 2003; doi10.1038/nmat1019

Keckes J, Burgert I, Müller M, Kölln K, Hamilton M, Burghammer M, Roth S, Stanzl-Tschegg S and Fratzl P (2004) In-situ synchrotron studies of structural changes in wood during microtensile tests. In: Stanzl-Tschegg SE, Gindl M and Sinn G (eds) Proc. of the 2nd Internat. symposium on Wood Machining, Vienna, Austria

Lichtenegger H, Reiterer A, Stanzl-Tschegg SE, Müller M, Paris O, and Fratzl P (2000). Cellulose orientation in the wood cell wall. In: Stanzl-Tschegg SE and Reiterer A, (eds) Proc Internat symposium on wood machining, Vienna, Austria; pp. 31–37

Morel S, Valentin G (1999) R-curve behaviour and roughness of wood fractured surfaces. Size effect. In: Damage in wood. COST E8. Mechanical performance of wood and wood products, Bordeaux, France

Niemz P (1993) Physik des Holzes und der Holzwerkstoffe. DRW-Verlag Leinfelden – Echterdingen

Petterson RP, Bodig J (1983) Prediction of Fracture Toughness of conifers. Wood Fib Sci 15(4):302–316

Reiterer A, Stanzl-Tschegg SE, Tschegg EK (2000) Mode I fracture and acoustic emission of softwood and hardwood. Wood Sci Techn 34:417–430

Reiterer A, Lichtenegger H, Fratzl P, Stanzl-Tschegg SE (2001) Deformation and energy absorption of wood cell walls with different nanostructure under tensile loading. J Mat Sci 36:4681–4686

Reiterer A, Sinn G, Stanzl-Tschegg SE (2002a) Fracture characteristics of different wood species under mode I loading perpendicular to the grain. Mat Sci Eng A332:29–36

Reiterer A, Burgert I, Sinn G., Tschegg SE (2002b) The radial reinforcement of the wood structure and its implication on mechanical and fracture mechanical properties – A comparison between two tree species. J Mat Sci 37: 935–940

Reiterer A, Tschegg SE (2002) The influence of moisture content on the mode I fracture behaviour of sprucewood. J Mat Sci 37:4487–4491

Schniewind AP, Ohgama T, Aoki T, Yamada T (1982) Effect of specific gravity, moisture content and temperature on fracture toughness of wood. Wood Sci 5(2):101–109

Schniewind AP, Pozniak RA (1971) On the fracture toughness of douglas fir wood. Eng Fract Mech 2:223–233

Stanzl-Tschegg SE, Tan D M, Tschegg EK (1995) New splitting method for wood fracture characterization. Wood Sci Techn 29:31–50

Tschegg EK (1986) Equipment and appropriate specimen shape for tests to measure fracture values (in German), Patent AT-390328

Valentin GH, Boström L, Gustafsson PJ, Ranta-Maunus A, Gowda S (1991) Application of fracture mechanics to timber structures RILEM state-of-the-art report. Technical Research Centre of Finland, Research Notes 1262